Multiple self-locking in the Kuramoto–Sakaguchi system with delay

Matthias Wolfrum[1], Serhiy Yanchuk[2], Otti D'Huys[3]

submitted: November 12, 2021

[1] Weierstrass Institute
     Mohrenstr. 39
     10117 Berlin
     Germany
     E-Mail: matthias.wolfrum@wias-berlin.de

[2] Technische Universität Berlin
     Institut für Mathematik
     Straße des 17. Juni 136
     10623 Berlin
     Germany
     E-Mail: yanchuk@math.tu-berlin.de

[3] Maastricht University
     Department of Data Science and Knowledge Engineering
     The Netherlands
     E-Mail: o.dhuys@maastrichtuniversity.nl

Multiple self-locking in the Kuramoto–Sakaguchi system with delay

Matthias Wolfrum, Serhiy Yanchuk, Otti D'Huys

Abstract

We study the Kuramoto-Sakaguchi system of phase oscillators with a delayed mean-field coupling. By applying the theory of large delay to the corresponding Ott–Antonsen equation, we explain fully analytically the mechanisms for the appearance of multiple coexisting partially locked states. Closely above the onset of synchronization, these states emerge in the Eckhaus scenario: with increasing coupling, more and more partially locked states appear unstable from the incoherent state, and gain stability for larger coupling at a modulational stability boundary. The partially locked states with strongly detuned frequencies are shown to emerge subcritical and gain stability only after a fold and a series of Hopf bifurcations. We also discuss the role of the Sakaguchi phase lag parameter. For small delays, it determines, together with the delay time, the attraction or repulsion to the central frequency, which leads to supercritical or subcritical behavior, respectively. For large delay, the Sakaguchi parameter does not influence the global dynamical scenario.

1 Introduction

In this paper, we study a system of Kuramoto-Sakaguchi phase oscillators with delayed global coupling. As an addition to earlier work on this system, we will use a combination of two tools: the Ott-Antonsen approach for the continuum limit of phase oscillator systems and the limit of large delay. This theory allows not only explicit analytical approximations of the stability problem for large delays but, at the same time, provides sufficient conditions for stability at any value of the delay.

Coupled oscillator systems appear in many fields of science, ranging from neuroscience and system biology to laser physics or economy [1, 2]. In many cases, their collective behavior can be described in terms of phase oscillators [3]. It has been shown in [4, 5, 6, 7, 8, 9] that the delay in the classical Kuramoto-Sakaguchi system leads to substantial modification of the dynamics. Time delays can be found in various applications, for a recent overview, see [10].

For large systems of coupled phase oscillators with sinusoidal coupling, the Ott-Antonsen approach [11, 12, 13, 14] allows the derivation of a dynamical equation for the order parameter, which is able to capture the collective dynamical regimes. Recently, also the version with time-delay has been studied in some detail. In particular, the paper [15] pointed out the importance of codimension two bifurcations, and [16] applied center manifold techniques to understand the bifurcation at the onset of synchronization.

Our goal is to provide a global picture of the dynamical regimes above the synchronization threshold. We present the model, and the corresponding Ott-Antonsen equation in Section 2. In Section 3, we revisit bifurcations of the partially locked states and organize them in a global picture. Next, in Section 4, we focus on the case of large delay. In particular, we show the appearance of an increasing number of coexisting locked states and bifurcation points. Using the limit of large delay [17, 18], we analytically investigate the stability properties of all partially locked states. It turns out that the coexisting stable

solutions are organized according to the Eckhaus scenario. This scenario is known originally from the classical Ginzburg-Landau setting [19], and it was transferred to systems with long-delayed feedback in [20]. The Eckhaus stability boundary for the set of stable partially locked states is given as modulational instability, which has been introduced to delay systems with large delay in [21, 22]. Finally, in Section 5, we summarize and discuss our results.

2   The model and Ott-Antonsen equation for the order parameter

We consider a population of N Kuramoto-Sakaguchi oscillators, coupled with a time-delay,

$$\dot{\phi}_k = \omega_k + \frac{\kappa}{N} \sum_{j=1}^{N} \sin\left(\phi_j(t - \tau) - \phi_k(t) + \alpha\right) , \tag{1}$$

with κ the coupling strength, τ the coupling delay, ω_k the natural frequency of the k-th oscillator and α the Sakaguchi phase lag parameter. Because of the sinusoidal coupling function, the system can be rewritten with the complex mean-field

$$r(t) = \eta(t)e^{i\Phi(t)} = \frac{1}{N} \sum_{j=1}^{N} e^{i\phi_j(t)} \tag{2}$$

as

$$\begin{align}
\dot{\phi}_k &= \omega_k + \kappa\eta(t - \tau)\sin\left(\Phi(t - \tau) - \phi_k(t) + \alpha\right) \tag{3} \\
&= \omega_k + \frac{\kappa}{2i}\left(r(t - \tau)e^{i(\alpha - \phi_k(t))} - \text{c.c.}\right) . \tag{4}
\end{align}$$

We assume the natural frequencies ω_k to be distributed according to the Lorentzian distribution

$$g(\omega) = \frac{1}{\pi(\omega^2 + 1)}. \tag{5}$$

Note that the width of the distribution has been rescaled to one; this can always be done by introducing an appropriate time scale in (1). Since the system is equivariant with respect to the S^1-symmetry of global phase shifts $\phi_i \to \phi_i + \psi$ for any real ψ, in the case without delay we can introduce a corotating frame $\phi_j \to \phi_i - \omega_0 t$, $\omega_j \to \omega_j + \omega_0$ and assume without further implications that the central frequency in (5) is equal to zero. However, when introducing a corotating frame in a system with a nonzero delay $\tau > 0$ we also have to adjust the phase shift parameter by $\alpha \to \alpha + \omega_0\tau$, i.e. it accounts now for the detuning from the case of resonant delay $\omega_0\tau = 2k\pi$.

In the limit of large number of oscillators [23], the oscillator population can be described by a probability density $f(\omega, \phi, t)$ governed by the Vlasov type continuity equation

$$\frac{\partial f}{\partial t} + \frac{\partial}{\partial \phi}(fv) = 0, \tag{6}$$

where the velocity v is given by the right hand side of (4), i.e.

$$v(\omega, \varphi, t) = \omega + \frac{\kappa}{2i}\left(r(t - \tau)e^{i(\alpha - \phi)} - \text{c.c.}\right) \tag{7}$$

with the integral version of the complex order parameter

$$r(t) = \int_{-\infty}^{+\infty} \int_0^{2\pi} f(\omega, \phi, t) e^{i\phi} \mathrm{d}\phi \mathrm{d}\omega. \tag{8}$$

For the system (6)–(8), E. Ott and T. Antonsen derived in [11] the following dynamical equation for the complex order parameter

$$\dot{r}(t) = -r + \frac{\kappa}{2} \left(e^{i\alpha} r(t-\tau) - e^{-i\alpha} \bar{r}(t-\tau) r^2(t) \right), \tag{9}$$

where they used the ansatz

$$f(\omega, \phi, t) = \frac{g(\omega)}{2\pi} \left(1 + \left(\sum z^n(\omega, t) e^{in\phi} + \mathrm{c.c.} \right) \right), \tag{10}$$

and the explicit solution of the integral

$$r(t) = \int g(\omega) \bar{z}(\omega, t) \mathrm{d}\omega = \bar{z}(-i, t) \tag{11}$$

for the Lorentzian frequency distribution (5).

3 Partially locked solutions and their bifurcations

3.1 Partially locked solutions

Partially locked solutions of the original oscillator model (1) correspond to solutions of the mean-field equation (9) of the form

$$r(t) = R e^{i\Omega t} \;\; \text{with} \;\; R \in [0, 1]. \tag{12}$$

Such solutions appear generically due to S^1-symmetry. It will turn out that, due to the delay, multiple stable coexisting partially locked solutions can emerge, with different frequencies, organized in a structure similar to a classical locking cone. Moreover, except for the central mode, i.e. the solution with its frequency closest to the mean frequency of the distribution (5), the partially locked solutions emerge unstable from the completely incoherent state and gain stability only after secondary bifurcations at a higher level of synchrony.

Inserting the ansatz (12) into (9), we obtain for the real and imaginary parts the conditions

$$\cos(\alpha - \Omega\tau) = \frac{2}{\kappa(1 - R^2)}, \tag{13}$$

$$\sin(\alpha - \Omega\tau) = \frac{2\Omega}{\kappa(1 + R^2)}. \tag{14}$$

Eliminating the trigonometric functions we get the expression

$$\left(\frac{\kappa}{2} \right)^2 = \frac{1}{(1 - R^2)^2} + \frac{\Omega^2}{(1 + R^2)^2}, \tag{15}$$

which gives a relation between frequencies Ω and amplitudes R of the partially locked solutions. Eliminating κ from (13), (14) we obtain the resonance condition

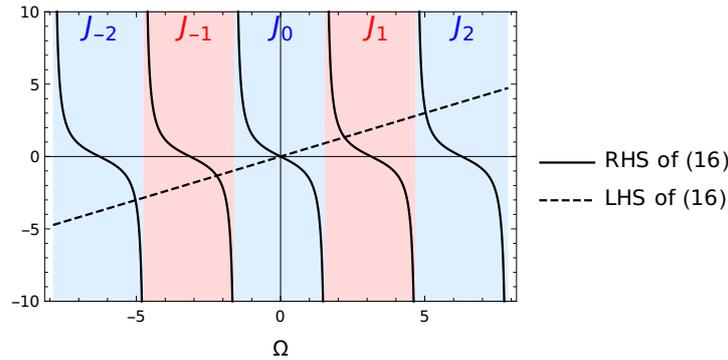$$\Omega = \frac{1 + R^2}{1 - R^2} \tan(\alpha - \Omega\tau), \tag{16}$$

Figure 1: Graphical solution of the resonance condition (16) for parameters $\alpha = 0$, $\tau = 1$, $R = 0.5$. The solutions Ω_k are given by the unique intersection of the solid and dashed line within each interval J_k (indicated by the shading). According to (13) solutions Ω_k with even k (blue shaded intervals) lead to positive κ while odd k (red shaded intervals) give a negative κ.

for the frequencies Ω. This transcendental scalar equation cannot be solved explicitly. However, for any given amplitude $R \in [0, 1]$ and fixed parameters $\tau > 0$, $\alpha \in [0, 2\pi]$ equation (16) has a unique solution $\Omega_k(R)$ within each interval

$$J_k = \left[\frac{2\alpha + (2k-1)\pi}{2\tau}, \frac{2\alpha + (2k+1)\pi}{2\tau} \right], \qquad k \in \mathbb{Z}, \tag{17}$$

see also Fig. 1. We observe that parameter α induces a shift of these intervals, while their length scales with $1/\tau$. For each $k \in \mathbb{Z}$ the corresponding solution branch $\Omega_k(R)$ of equation (16) can be obtained numerically. Then, (13) directly provides the corresponding values $\kappa_k(R)$. From the sign of the cosine in equation (13) we conclude that these solution branches provide uniformly either positive or negative values of κ, alternatingly for even and odd values of k. Since the system is invariant under the transformation $\kappa \mapsto -\kappa, \alpha \mapsto \alpha + \pi$, we can restrict ourselves to the case $\kappa \geq 0$ and only consider even values of k, i.e. solutions to (13) in the blue regions in Fig. 1. Note that $R \to 1$ implies $|\kappa_k(R)| \to \infty$, while at $R = 0$ the branches of rotating wave solutions (12) end at a finite value $\kappa_k(0)$ where they bifurcate from the zero solution.

3.2 Hopf bifurcations of partially locked solutions

Inserting $R = 0$ into (15) we obtain the frequency-dependent synchronization threshold

$$\left(\frac{\kappa}{2} \right)^2 = 1 + \Omega^2, \tag{18}$$

which is a necessary condition for a purely imaginary eigenvalue of the linearization of equation (9) at the zero solution. Note that the synchronization threshold (18) does not depend on τ and α. The Hopf frequencies $\Omega_k(0)$ can be obtained from the resonance condition (16) which for $R = 0$ reduces to

$$\Omega = \tan(\alpha - \Omega\tau), \tag{19}$$

while from (13) we obtain the corresponding coupling strengths

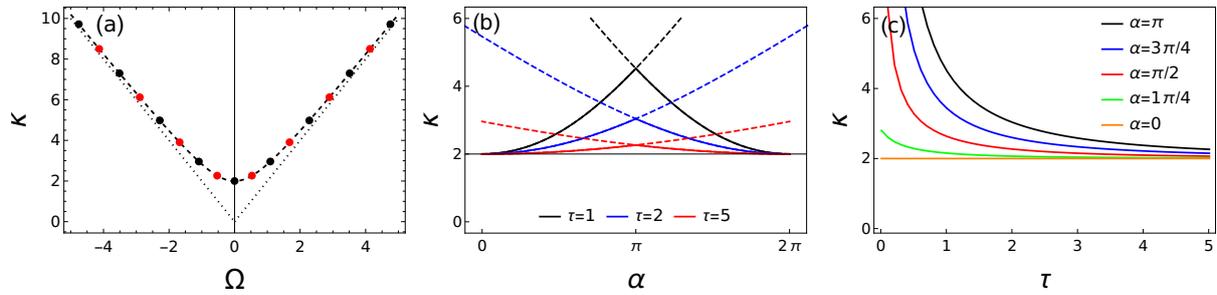$$\kappa_k(0) = \frac{2}{\cos(\alpha - \tau\Omega_k(0))}.$$

Figure 2: (a) Dashed line: frequency dependent synchronization threshold (18). Dotted line: asymptotic linear cone. Black dots: Hopf bifurcations $(\Omega_k(0), \kappa_k(0))$ of partially locked solutions for $\tau = 5$ and $\alpha = 0$. Red dots: Hopf bifurcations for $\tau = 5$ and $\alpha = \pi$. (b) Onset of partial synchrony at $\kappa_0(0)$ (primary Hopf bifurcation) for varying α and different choices of τ according to (20). (c) Onset of partial synchrony at $\kappa_0(0)$) for varying τ and different choices of α. In (b) and (c) the incoherent state is stable in the parameter region below the corresponding solid line.

Recall that without loss of generality we may restrict ourselves to positive $kappa$, which corresponds to even values k. For $\alpha = 0$, the primary Hopf bifurcation, where the incoherent solution $r(t) = 0$ loses its stability, occurs at the central frequency $\Omega = 0$ and at the classical Kuramoto threshold $\kappa = 2$, independent of the delay. However, due to the delay, synchrony can emerge for all values of α, including those corresponding to repulsive coupling. In such cases, the locking frequency Ω is detuned from the central frequency, and the onset of partial synchrony happens at a higher value of κ. The mechanism for synchronization at repulsive coupling can be explained as follows: the oscillators are repelled from the *delayed* position of the mean field but, for positive delay and properly detuned frequency, it can happen that at the same time they are pushed towards the *instantaneous* position of the mean field.

Figure 2(a) shows the frequency-dependent synchronization threshold (18) and the Hopf bifurcations for $\alpha = 0, \pi$, and $\tau = 5$. One can see that the synchronization threshold behaves asymptotically like a linear locking cone. With changing α, the Hopf points move along the curve (18), while for larger τ they become more densely distributed. One can see that, for $\alpha = \pi$, the zero state $r = 0$ of complete incoherence loses its stability with increasing κ in a double Hopf bifurcation, where two Hopf bifurcations with frequencies Ω and $-\Omega$ occur simultaneously. This is because the complex conjugation $r \mapsto \bar{r}$ is a symmetry of equation (9) for $\alpha = 0$ and $\alpha = \pi$. In both cases, $\alpha = 0$ and $\alpha = \pi$, all secondary Hopf bifurcations, where unstable partially locked states bifurcate from the already unstable zero solution, are double ones, caused by this symmetry.

In order to obtain the relation between α and the coupling strength κ at the primary Hopf bifurcation, corresponding to the onset of partial synchrony, one can combine equations (18) and (19) to

$$\alpha = \pm \left(\arctan \sqrt{\left(\frac{\kappa}{2}\right)^2 - 1} + \tau \sqrt{\left(\frac{\kappa}{2}\right)^2 - 1} \right) + 2k\pi. \tag{20}$$

Figure 2(b) shows these curves in the (κ, α) parameter plane for different choices of delay τ. At $\alpha = \pi$ the onset of synchrony happens at a maximal value of $\kappa_0(0)$, and the two leading modes interchange their order.

Figure 2(c) shows the same bifurcations in the parameter plane (τ, κ) for different values of α. Note that, according to (20), for $\pi/2 \leq \alpha \leq 3\pi/2$ and $\tau \to 0$, the threshold value $\kappa_0(0)$ tends to infinity, while it remains finite for $|\alpha| < \pi/2$, i.e. in the case of attractive coupling.
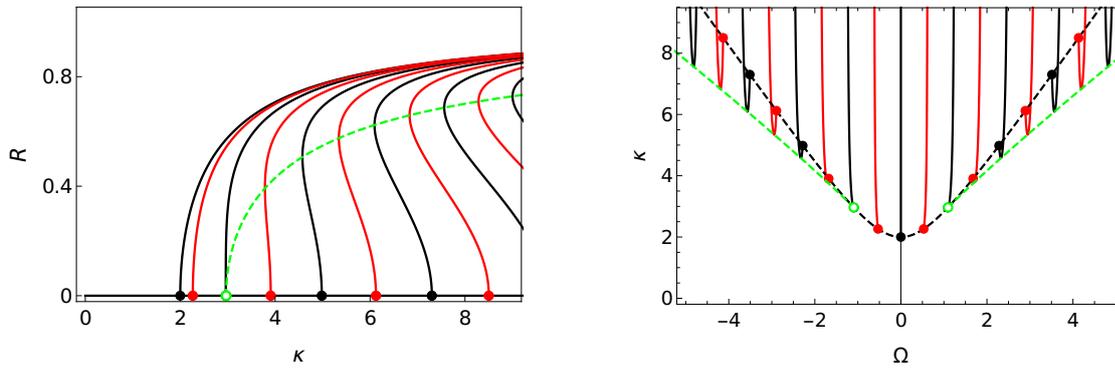
Figure 3: Branches of partially locked states with Hopf bifurcations for $\tau = 5$. Black: Branches and Hopf points for $\alpha = 0$. Red: Branches and Hopf points for $\alpha = \pi$. Green curve: Location of folds according to (23), (24). Green circles: degenerate Hopf at (25), (26).

3.3   Branches of partially locked solutions and fold bifurcations

In Fig. 3 we show numerically computed branches of partially locked solutions (12) for fixed $\tau = 5$ and $\alpha = 0$, π and varying $\kappa > 0$. We observe that beyond a certain coupling strength, the branches bifurcate subcritically from the zero solution, before they turn back in a fold bifurcation. This fold can be calculated as follows. Eliminating R from (13) and (14) we get the condition

$$\Omega = \kappa \sin(\alpha - \Omega\tau) - \tan(\alpha - \Omega\tau), \tag{21}$$

which we differentiate with respect to Ω in order to obtain double roots at

$$\kappa = \frac{1}{\cos^3(\alpha - \Omega\tau)} - \frac{1}{\tau \cos(\alpha - \Omega\tau)}. \tag{22}$$

Using (13), (15), and (22) we obtain the location of the folds

$$\left(\frac{\kappa}{2}\right)^2 = \frac{2}{(1 - R^2)^3} + \frac{1}{\tau(1 - R^2)^3}, \tag{23}$$

$$\Omega^2 = \left(\frac{1 + R^2}{1 - R^2}\right)^3 + \frac{1}{\tau}\left(\frac{1 + R^2}{1 - R^2}\right)^2. \tag{24}$$

Together with the resonance condition (13), these expressions provide the folds for each branch of partially locked states. The green dashed curves in Figure 3 are given by (23) and (24), and meet the branches of partially locked states precisely at the fold points. Note that the fold curves terminate for $R = 0$ at the point

$$\kappa = 2\sqrt{2 + 1/\tau}, \tag{25}$$

$$\Omega = \pm\sqrt{1 + 1/\tau} \tag{26}$$

such that branches of partially locked states emerging with a Hopf frequency $|\Omega| < \pm\sqrt{1 + 1/\tau}$ have no fold and bifurcate supercritically. If Ω in (26) also satisfies the resonance condition (19), then the corresponding branch emerges from the zero solution in a degenerate Hopf (Bautin) bifurcation, which is characterized by a transition from super- to subcritical behavior. Combining (26) and (19) we obtain for the Bautin points the condition

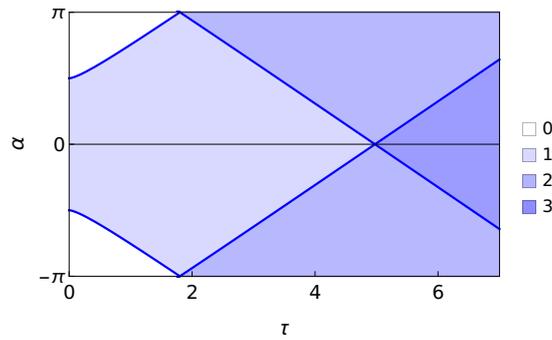$$\alpha = \pm\left(\arctan\left[\sqrt{1 + 1/\tau}\right] + \sqrt{\tau^2 + \tau}\right) + 2k\pi. \tag{27}$$

Figure 4: Regions the (τ, α) parameter plane with different numbers of supercritical branches, given by (27). In the white region, for increasing κ all branches of partially locked solutions bifurcate subcritically from the zero solution and, hence, the onset of partial synchronization happens in a first order (subcritical) transition. For larger delay τ there is an increasing number of supercritical branches.

In particular, we conclude that for small values of $\tau > 0$ and α close to π, the primary branch of partially locked states emerges beyond the Bautin points and hence behaves subcritical, i.e., the onset of synchronization behaves like a first-order transition. Note that according to (25) this happens for rather large values of κ. In Figure 4 we show how the number of supercritical branches increases for increasing τ. Only in the white region, there are no supercritical branches, and already the primary branch behaves subcritical. For the parameters chosen in Figure 3, there are two supercritical branches in the case $\alpha = \pi$ and three at $\alpha = 0$. In the latter case, our choice $\tau = 5$ by coincidence almost exactly hits the Bautin point, which can be calculated by (27) to happen at $\alpha \approx 4.97494$.

4 Stability of partially locked solutions in the large delay limit

We have seen that in the situation of larger values of τ there is an increasing number of branches of partially locked states. However, all secondary branches bifurcate unstable from the already unstable zero solution. In order to investigate how these branches eventually gain stability, we will invoke the stability theory in the limit of large delay [17]. This theory can provide explicit analytical expressions for the stability at infinite delay, which not only provide good approximations for the case of large finite delay, but can also give sufficient conditions for the stability at any finite delay.

First we recall that the frequency dependent synchronization threshold (18) is already independent on τ and α. Moreover, the bifurcation condition (22) for the fold has a straightforward version for large values of τ given by

$$\kappa = \frac{1}{\cos^3(\alpha - \Omega\tau)}, \tag{28}$$

from which we derive the condition

$$R = \sqrt{1 - 2\kappa^{-2/3}}, \tag{29}$$

which is now also independent on τ and α. Using (15), this gives an explicit condition for the frequencies

$$\Omega = \left(\kappa^{2/3} - 1\right)^{3/2}, \tag{30}$$

i.e. we have already some information about the existence region of partially locked solutions in the case of large delay.

In the case of large delay, the frequencies Ω of the partially locked states become denser and can be treated as a pseudo-continuous family. Indeed, as follows from (17), the distance between the neighboring roots Ω_k is proportional to $1/\tau$. Hence, for $\tau \to \infty$, also the curves of Hopf and fold bifurcations will be filled densely with bifurcation points, see Fig. 3(b).

4.1   Large delay limit and stability of the incoherent solution

In order to analyze the stability of the partially locked solutions, we briefly recall some basic facts from [17] about the spectral theory of delay systems with large delay. For a linear system of the form

$$\dot{\vec{v}}(t) = A\vec{v}(t) + B\vec{v}(t - \tau) \tag{31}$$

with coefficient matrices A and B, the eigenvalue spectrum shows certain scaling properties for $\tau \to \infty$. The asymptotic location of the spectrum can be calculated and provides a good approximation for the exact spectrum at large finite values of τ. The onset of instability is governed by the so-called *pseudo-continuous spectrum*, which can be calculated by inserting the ansatz $\lambda = \varepsilon\gamma + i\sigma$, $\varepsilon = 1/\tau$, into the characteristic equation

$$\chi(\lambda) = \det(\lambda\mathrm{Id} - A - e^{-\lambda\tau}B) = 0, \tag{32}$$

and omitting terms of order ε. Replacing the term $e^{\gamma + i\sigma\tau}$ by Y, we obtain the equation

$$\det(i\sigma\mathrm{Id} - A - YB) = 0. \tag{33}$$

This is a polynomial in Y with degree $\mathrm{rank}(B) > 0$. For each branch of complex roots $Y_*(\sigma)$ of this polynomial, we obtain a spectral curve

$$\gamma_*(\sigma) = -\ln\left(|Y_*(\sigma)|\right)$$

determining real parts of the eigenvalues for large τ. More precisely, the eigenvalues accumulate along the curve $\lambda = \varepsilon\gamma_*(\sigma) + i\sigma$. For the detailed theoretical background of this procedure, see [17].

We now apply this procedure to equation (9). When we linearize (9), we must split it into real and imaginary parts $r = x + iy$ in order to deal with the complex conjugation. Hence, the characteristic equation (33) contains real 2×2 matrices and there are generically two branches of complex roots $Y_{1,2}(\sigma)$. The polynomial (33) can be rewritten as

$$D_B Y^2 + (C - i\sigma T_B)Y + D_A - i\sigma T_A - \sigma^2 = 0, \tag{34}$$

where $D_{A,B}$ denote the determinants and $T_{A,B}$ the traces of the matrices A and B, respectively. Additionally, we have introduced

$$C = \det(A + B) - D_A - D_B.$$

The linearization at the zero solution gives the matrices

$$A = \begin{pmatrix} -1 & 0 \\ 0 & -1 \end{pmatrix}, \qquad B = \frac{\kappa}{2}\begin{pmatrix} \cos\alpha & -\sin\alpha \\ \sin\alpha & \cos\alpha \end{pmatrix}. \tag{35}$$

With matrices (35), the polynomial (34) possesses the roots

$$Y_{1,2}(\sigma) = \frac{2}{\kappa}(1 + i\sigma)e^{\pm i\alpha}.$$

Due to the specific form of the equation, this results in the single branch of pseudo-continuous spectrum

$$\gamma_*(\sigma) = \ln\left(\frac{\kappa}{2}\right) - \frac{1}{2}\ln\left(1 + \sigma^2\right).$$
(36)

The expression (36) shows that the onset of partial synchrony at $\kappa = 2$ is expressed as an instability of the pseudo-continuous spectrum with the real part of the eigenvalue $\gamma_*(\sigma)$ becoming positive at $\sigma = 0$. Such a scenario has been studied in detail for Stuart-Landau oscillators with long-delayed feedback in [20]. It has been shown that locally this instability can be described in terms of the Eckhaus scenario, which is originally known from the classical real Ginzburg-Landau equation. In that setup, the critical spectrum is locally approximated by a parabola, and the zero solution becomes unstable with respect to periodic patterns. Within the band of unstable wavenumbers from the zero solution, there is the region of coexisting Eckhaus stable periodic patterns, which also has a parabolic shape covering precisely two-thirds of the unstable wavenumbers of the zero solution. For the oscillatory instability with large delay, there is a similar scenario of coexisting time-periodic solutions. They emerge at the frequency-dependent synchronization threshold (18), which can be approximated by a parabola locally around the central frequency $\Omega = 0$. The solution at the central frequency bifurcates stable, while the solutions with side-band frequencies $\Omega \neq 0$ emerge unstable, and gain stability at the *Eckhaus stability boundary*, which is locally also given by a parabola. However, we do not content ourselves here with the local parabolic approximation but calculate the exact location of the Eckhaus stability boundary for distant frequencies.

4.2 Stability of partially locked solutions

In order to calculate the pseudo-continuous spectrum of the partially locked solutions (12), we introduce the corotating coordinate frame $r_{\text{new}} = re^{-i\Omega t}$ and split the equation into real and imaginary parts $r_{\text{new}} = x + iy$. This gives the real system

$$\begin{aligned}
\dot{x} = &- x + \Omega y + \frac{\kappa}{2}[(\cos(\alpha - \Omega\tau)x_\tau - \sin(\alpha - \Omega\tau)y_\tau)(1 - x^2 + y^2) \\
&- 2xy(\sin(\alpha - \Omega\tau)x_\tau + \cos(\alpha - \Omega\tau)y_\tau)]
\end{aligned}$$
(37)

$$\begin{aligned}
\dot{y} = &- \Omega x - y + \frac{\kappa}{2}[(\sin(\alpha - \Omega\tau)x_\tau + \cos(\alpha - \Omega\tau)y_\tau)(1 + x^2 - y^2) \\
&- 2xy(\cos(\alpha - \Omega\tau)x_\tau - \sin(\alpha - \Omega\tau)y_\tau)],
\end{aligned}$$
(38)

where we used the abbreviations $x_\tau = x(t - \tau)$, $y_\tau = y(t - \tau)$. The partially locked solutions, given by the conditions (13) and (14), appear as one-parameter families of stationary states $x + iy = Re^{i\varphi}$, $\varphi \in S^1$. From these we choose $\varphi = 0$, i.e., $x = R$, $y = 0$ and obtain for the corresponding linearization of (9) in the form (31) the matrices

$$A = \begin{pmatrix} -q & \Omega/q \\ -\Omega/q & -q \end{pmatrix}, \qquad B = \begin{pmatrix} 1 & -\Omega/q \\ \Omega & q \end{pmatrix}$$
(39)

with

$$q = \frac{1 + R^2}{1 - R^2}.$$

Examples of pseudo-continuous spectra of partially locked solutions with different parameters are given in Fig. 5.

Since the locked states appear as families of stationary states, we always get a trivial eigenvalue $\lambda = 0$, corresponding to the tangential direction along the family. This implies that for one of the
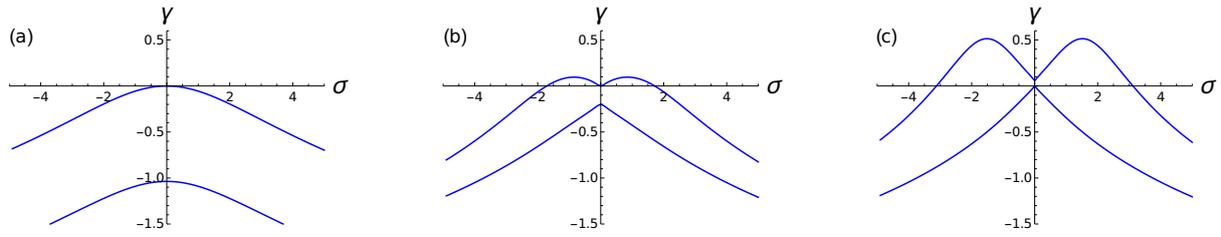
Figure 5: Pseudo-continuous spectrum of coexisting partially locked solutions at $\kappa = 4$: (a) – spectrum of stable solution with $R = 0.7$ and resulting $\Omega = 0.5872$; (b) – spectrum of modulationally unstable solution with $R = 0.55$ and resulting $\Omega = 1.8162$; (c) – spectrum of uniformly unstable solution with $R = 0.3$ and resulting $\Omega = 1.8214$. Note that for large but finite τ the existence region is densely filled with solution branches such that partially locked solutions with prescribed amplitude R can always be found by small variations in α or τ.

two curves, we have $\gamma_*(0) = 0$. The main destabilization mechanism is a so-called modulational instability, which is characterized by the fact that the critical curve of the pseudo-continuous spectrum with $\gamma_*(0) = 0$ changes its curvature at $\omega = 0$, i.e., $\gamma_*''(0) = 0$. This scenario has been described for delay systems with large delay in [20, 24].

Theorem 1. *For the partially locked solutions (12) of equation (9) in the limit of $\tau \to \infty$ the condition for modulational instability is given by*

$$\Omega^2 = \kappa^2 - \sqrt[3]{32}\kappa^{4/3} + \frac{\sqrt[3]{250}}{2}\kappa^{2/3} - 1. \tag{40}$$

Moreover, the stability region delineated by (40) provides a sufficient condition for stability of partially locked solutions (12) valid for all positive delays $\tau > 0$ (absolute stability).

The following lemma shows, how for systems of two real equations, such as as (37)–(38), the condition for modulational instability can be calculated in terms of the matrices of the linearization.

Lemma 1. *A linear delay system of the form*

$$\dot{\vec{v}} = A\vec{v} + B\vec{v}_\tau \tag{41}$$

with real 2×2 matrices A and B satisfying

$$\det(A + B) = 0 \tag{42}$$

has in the limit of large delay a critical branch of the pseudo-continuous spectrum undergoing a modulational instability if

$$(D_A - D_B)^2 + (T_A + T_B)(D_A - D_B)T_B - \frac{1}{2}(T_A + T_B)^2(D_A - 3D_B) = 0 \tag{43}$$

is satisfied. By $D_{A,B}$ we denote the determinants and by $T_{A,B}$ the traces of the matrices A and B, respectively.

Proof: For real 2×2 matrices A and B in (41) there are two branches of pseudo-continuous spectrum

$$\gamma_{1,2}(\sigma) = -\ln\left(|Y_{1,2}(\sigma)|\right),$$

originating from the roots $Y_{1,2}$ of the polynomial (34). The condition (42) implies that $(Y, \sigma) = (1, 0)$ is a solution of (34) and we obtain a critical branch of the pseudo-continuous spectrum with $\gamma_{\mathrm{crit}}(0) = 0$. Implicit differentiation of (34) with respect to σ gives

$$-2\sigma - i(T_A + YT_B) - i\sigma Y'T_B + 2YY'D_B + Y'C = 0. \tag{44}$$

Inserting $Y = 1$, $\sigma = 0$ and the condition (42) we obtain

$$Y'(0) = -i\frac{T_A + T_B}{D_A - D_B}. \tag{45}$$

A second implicit differentiation gives

$$-2 - 2iY'T_B - i\sigma Y'' + 2\left(YY'' + Y'^2\right)D_B + Y''C = 0. \tag{46}$$

Inserting $Y = 1$, $\sigma = 0$, (42), and (45), we get

$$Y''(0) = -2\frac{(D_A - D_B)^2 + (T_A + T_B)(D_A - D_B)T_B + (T_A + T_B)^2 D_B}{(D_A - D_B)^3}. \tag{47}$$

The condition for modulational instability $\gamma''(0) = 0$ is satisfied if the second derivative of $|Y(0)|$ vanishes. Taking into account that $Y''(0)$ is real, this leads to $Y''(0) - |Y'(0)|^2 = 0$. Using (47) and (45), this gives the condition (43) stated in the lemma.

$$\square$$

With this lemma we can now proceed to prove the theorem: Using the expressions for the matrices (39) and the condition (43), we obtain for the modulational instability of the partially locked states

$$\Omega^2 = \frac{q^2(q-1)}{2}. \tag{48}$$

Rewriting (15) in terms of q and inserting (48) we obtain for the coupling strength at the modulational instability

$$\kappa^2 = \frac{(q+1)^3}{2}. \tag{49}$$

Equations (48) and (49) can be combined to the bifurcation condition (40) given in the theorem.

The fact that stability for large delay implies stability for all positive values of the delay (absolute stability) can be seen as follows: Assume that for some finite delay $\tau_0 > 0$, coupling strength $\kappa > 2$, and some choice of α_0 there is a partially locked solution (12) with frequency Ω and amplitude R that within the stability region delineated by the stability boundary (40), which we derived for the case of infinite delay. Moreover, assume that this solution, written as a stationary solution in a corotating frame, has at least one unstable eigenvalue λ_0. If we now increase the delay and adapt α by

$$\alpha(\tau) = \alpha_0 + \Omega(\tau - \tau_0),$$

then according to (13), (14) this solution will persist, i.e. Ω and R will stay constant. Since we keep also κ fixed, the solution will keep its position fixed within the stability region for large delay. In this way we can reach arbitrarily large values of τ, where the solution is known to be stable. Hence, the unstable eigenvalue $\lambda(\tau)$ has to cross the imaginary axis for some intermediate value $\hat{\tau}$. With a purely imaginary eigenvalue $\lambda = i\hat{\sigma}$ as a solution of the characteristic equation (32), also $\hat{Y} = e^{i\hat{\sigma}\hat{\tau}}$ together
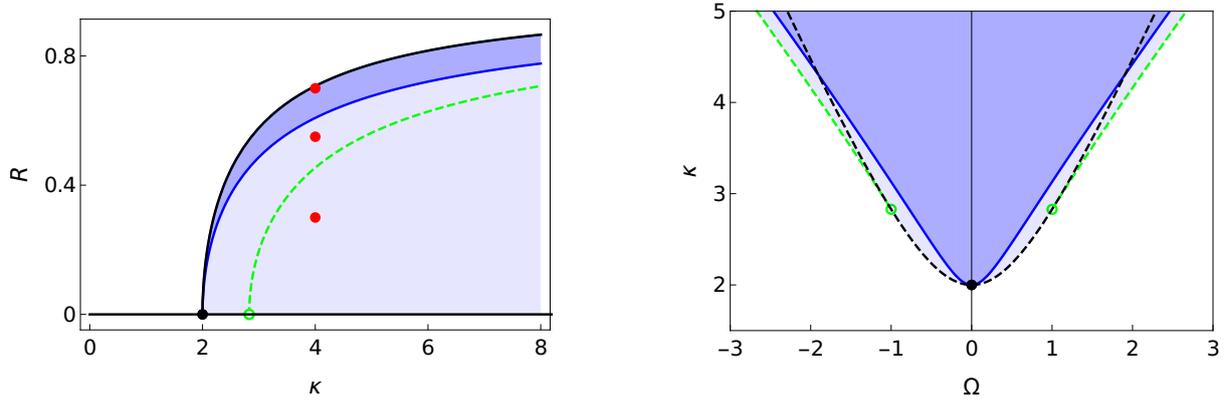
Figure 6: Shaded regions indicate existence (light) and stability (dark) of partially locked states in the limit of large delay. Blue curve: modulational instability (40). Green dashed curves: folds of partially locked states (29), (30), ending at degenerate Hopf (green circles). Black dashed curve in panel (b): frequency dependent synchronization threshold (18). Pseudo-continuous spectrum of partially locked states at red dots in panel (a) is shown in Fig. 5.

with $\hat{\sigma}$ solves the equation (33) for the pseudo-continuous spectrum and the corresponding branch satisfies $\gamma(\hat{\sigma}) = 0$. However, the whole pseudo-continuous spectrum was assumed to be stable and only the critical branch touches the imaginary axis at $\sigma = 0$. The corresponding trivial eigenvalue, which exists due to the rotation symmetry, is fixed, and it cannot move into the unstable half plane. If there would be another eigenvalue at zero, the parameters would have to satisfy the fold condition (23). But it can be easily seen that the fold curve does never enter the Eckhaus stable region. This shows by contradiction that for a partially locked solution within the Eckhaus stable region stability for large delay implies stability for all positive τ and all choices of α. This completes the proof of the theorem.

$\square$

The results for the case of large delay are summarized in Figure 6, showing the regions of existence and stability of the coexisting partially locked states together with the modulational instability and the fold curves. The fold curve is located within the unstable region; when crossing this curve, the pseudo-continuous spectrum changes its shape. Indeed, we observe that according to (45) and (47) the first and second derivatives of Y, and hence of the critical curves of pseudo-continuous spectrum γ, have a singularity at $\sigma = 0$ if the denominator $D_A - D_B$ vanishes. This coincides with fold condition (24), which in the limit of large delay, can be rewritten as $\Omega^2 = q^3$. As a result, the fold curve induces a branch switching singularity of the pseudo-continuous spectrum, mediating between the two different types of pseudo-continuous spectrum given in Figure 5(b) and (c). Moreover, at the fold, we have another eigenvalue at zero, additionally to the trivial eigenvalue from the phase shift of the partially locked states. This leads to a degeneracy $\gamma_1(0) = \gamma_2(0) = 0$ of the two curves of the pseudo-continuous spectrum at zero, the role of the critical branch switches, and a transition from modulationally unstable to uniformly unstable partially locked states occurs. The fold curves terminate at degenerate points (green dots in Fig. 6) where this change of instability happens on the frequency dependent synchronization threshold (18) and, at the same time, the branches of partially locked states change between supercritical and subcritical.

5 Discussion and Outlook

Our results describe partially locked states in a large population of Sakaguchi-Kuramoto oscillators with delayed coupling. Moreover, in many cases, we can provide analytic expressions for the dynamics, instabilities, and bifurcations. In contrast to the Sakaguchi-Kuramoto oscillator system without delay, the delay is known to induce the following two important differences [4, 5]:

(i) Synchronization can also emerge for repulsive coupling, i.e., for $\pi/2 < \alpha < 3\pi/2$, and sometimes emerges subcritical.

(ii) There are multiple coexisting stable partially locked states.

We have shown that the onset of synchronization can be described by a frequency-dependent synchronization threshold. This threshold is independent of the phase lag and the delay, and it describes how partially locked states with larger detuning from the central frequency emerge for larger coupling. Along this threshold curve, there are two Bautin points, beyond which branches with sufficiently large detuning bifurcate subcritical, see Fig. 3. The role of the phase lag parameter α has to be reinterpreted as the detuning from the resonant delay and becomes less important in the case of larger delay, where there are more resonances closer to each other.

In the case of large delay, this results in an increasing number of coexisting stable partially locked states. We investigated their stability by methods of the large delay limit. It can be shown that close to the onset of partial synchrony, they are organized according to the classical Eckhaus scenario, which has already been described for other oscillatory systems with delayed feedback. As a characteristic feature of this scenario, only the partially locked state closest to the central frequency emerges stable from the zero solution. In contrast, the partially locked states at detuned frequencies gain stability with nonzero amplitude at the Eckhaus boundary of modulational instability. The specific structure of the Ott-Antonsen equation allows us to perform this stability analysis not only locally around the central frequency, but globally for all frequencies. As a result, we obtain a stability region, which rather resembles a locking cone than the typical parabolic Eckhaus stability region. Moreover, in the global scenario (see Fig. 6) with the Bautin points and the subcritical branches, the stability region extends below the frequency-dependent synchronization threshold, such that stable partially locked states exist at frequencies, with respect to which the zero solution is stable.

A key ingredient of our approach is the restriction to Lorentzian frequency distributions. Without this restriction, new effects arise, see, e.g. [25] for the case of bimodal distributions. Nevertheless, even for unimodal distributions, the situation can be more complicated. Indeed already without delay, an interplay of the phase lag and certain unimodal frequency distributions can lead to a variety of non-universal synchronization transitions, including subcritical and nonmonotonic behavior [26, 27, 28].

At the other hand, already a single oscillator with delayed self-coupling gives rise to multiple coexisting stable self-locked solutions. This situation has been studied in [29] together with the influence of noise. The observed effect of stochastic switching towards the central frequency is likely to happen similarly in our case of a globally coupled ensemble under the influence of noise. A related question is the behavior for random initial conditions and the relative size of the basins for the different resonant frequencies. Following the results in [30], where this question has been addressed for coexisting states with different wave numbers in a spatially extended system of coupled phase oscillators, one would expect as well a strong bias towards the central part of the stable frequencies.

When considering delay coupled oscillatory systems beyond phase oscillators, the amplitude can play an important role and induce new dynamical phenomena already in small systems [31]. It might be

an interesting question to understand the amplitude effects in a globally delay coupled heterogeneous oscillator population on the dynamical scenario presented here.

References

[1] A. T. Winfree, The Geometry of Biological Time, Vol. 12, Springer, 2001. `arXiv:arXiv:1011.1669v3`, `doi:10.1007/978-1-4757-3484-3`.
URL `http://link.springer.com/10.1007/978-1-4757-3484-3`

[2] A. Pikovsky, M. Rosenblum, J. Kurths, Synchronization: A Universal Concept in Nonlinear Sciences, Cambridge Nonlinear Science Series, Cambridge University Press, 2001. `doi:10.1017/CBO9780511755743`.

[3] H. Sakaguchi, Y. Kuramoto, A soluble active rotator model showing phase transitions via mutual entrainment, Prog. of Theor. Phys. 76 (3) (1986) 576–581. `arXiv:https://academic.oup.com/ptp/article-pdf/76/3/576/5302137/76-3-576.pdf`, `doi:10.1143/PTP.76.576`.
URL `https://doi.org/10.1143/PTP.76.576`

[4] M. K. S. Yeung, S. H. Strogatz, Time delay in the Kuramoto model of coupled oscillators, Phys. Rev. Lett. 82 (1999) 648–651. `doi:10.1103/PhysRevLett.82.648`.
URL `https://link.aps.org/doi/10.1103/PhysRevLett.82.648`

[5] M. Y. Choi, H. J. Kim, D. Kim, H. Hong, Synchronization in a system of globally coupled oscillators with time delay, Phys. Rev. E 61 (2000) 371–381. `doi:10.1103/PhysRevE.61.371`.
URL `https://link.aps.org/doi/10.1103/PhysRevE.61.371`

[6] T. K. D. Peron, F. A. Rodrigues, Explosive synchronization enhanced by time-delayed coupling, Physical Review E 86 (1) (2012) 016102. `arXiv:1110.5377`, `doi:10.1103/PhysRevE.86.016102`.
URL `https://journals.aps.org/pre/abstract/10.1103/PhysRevE.86.016102https://link.aps.org/doi/10.1103/PhysRevE.86.016102`

[7] A. Nordenfelt, A. Wagemakers, M. A. F. Sanjuán, Frequency dispersion in the time-delayed Kuramoto model, Physical Review E 89 (3) (2014) 032905. `doi:10.1103/PhysRevE.89.032905`.
URL `https://journals.aps.org/pre/abstract/10.1103/PhysRevE.89.032905https://link.aps.org/doi/10.1103/PhysRevE.89.032905`

[8] H. Wu, L. Kang, Z. Liu, M. Dhamala, Exact explosive synchronization transitions in Kuramoto oscillators with time-delayed coupling, Scientific Reports 8 (1) (2018) 15521. `doi:10.1038/s41598-018-33845-6`.
URL `www.nature.com/scientificreports/http://www.nature.com/articles/s41598-018-33845-6`

[9] I. Al-Darabsah, S. A. Campbell, A phase model with large time delayed coupling, Physica D: Nonlinear Phenomena 411 (2020) 132559. `doi:10.1016/j.physd.2020.132559`.
URL `https://linkinghub.elsevier.com/retrieve/pii/S0167278919306426`

[10] T. Erneux, J. Javaloyes, M. Wolfrum, S. Yanchuk, Introduction to Focus Issue: Time-delay dynamics, Chaos: An Interdisciplinary Journal of Nonlinear Science 27 (11) (2017) 114201. `arXiv:` `https://doi.org/10.1063/1.5011354,doi:10.1063/1.5011354.`
URL `https://doi.org/10.1063/1.5011354`

[11] E. Ott, T. M. Antonsen, Low dimensional behavior of large systems of globally coupled oscillators, Chaos: An Interdisciplinary Journal of Nonlinear Science 18 (3) (2008) 037113. `arXiv:` `https://doi.org/10.1063/1.2930766,doi:10.1063/1.2930766.`
URL `https://doi.org/10.1063/1.2930766`

[12] E. Ott, T. M. Antonsen, Long time evolution of phase oscillator systems, Chaos: An Interdisciplinary Journal of Nonlinear Science 19 (2) (2009) 023117. `arXiv:https://doi.org/` `10.1063/1.3136851,doi:10.1063/1.3136851.`
URL `https://doi.org/10.1063/1.3136851`

[13] W. S. Lee, E. Ott, T. M. Antonsen, Large coupled oscillator systems with heterogeneous interaction delays, Phys. Rev. Lett. 103 (4) (2009) 44101. `doi:10.1103/PhysRevLett.103.` `044101.`
URL `http://link.aps.org/doi/10.1103/PhysRevLett.103.044101`

[14] C. Bick, M. Goodfellow, C. R. Laing, E. A. Martens, Understanding the dynamics of biological and neural oscillator networks through exact mean-field reductions: a review, J. Math. Neurosci. 10 (1) (2020) 9. `doi:10.1186/s13408-020-00086-9.`
URL `https://mathematical-neuroscience.springeropen.com/` `articles/10.1186/s13408-020-00086-9`

[15] B. Niu, Codimension-two bifurcations induce hysteresis behavior and multistabilities in delay-coupled Kuramoto oscillators, Nonlinear Dynamics `doi:10.1007/` `s11071-016-3078-5.`

[16] D. Métivier, S. Gupta, Bifurcations in the time-delayed Kuramoto model of coupled oscillators: Exact results, J. of Stat. Phys. 176 (2019) 279–298.

[17] M. Lichtner, M. Wolfrum, S. Yanchuk, The spectrum of delay differential equations with large delay, SIAM Journal on Mathematical Analysis 43 (2) (2011) 788–802. `arXiv:https://` `doi.org/10.1137/090766796,doi:10.1137/090766796.`
URL `https://doi.org/10.1137/090766796`

[18] S. Yanchuk, L. Lücken, M. Wolfrum, A. Mielke, Spectrum and amplitude equations for scalar delay-differential equations with large delay, Discrete & Continuous Dynamical Systems - A 35 (1) (2015) 537–553. `doi:10.3934/dcds.2015.35.537.`
URL `http://aimsciences.org//article/id/a78a46dc-43d4-42a6-9e23-aab5e865`

[19] L. S. Tuckerman, D. Barkley, Bifurcation analysis of the eckhaus instability, Physica D: Nonlinear Phenomena 46 (1) (1990) 57 – 86. `doi:https://doi.org/10.1016/` `0167-2789(90)90113-4.`
URL `http://www.sciencedirect.com/science/article/pii/` `0167278990901134`

[20] M. Wolfrum, S. Yanchuk, Eckhaus instability in systems with large delay, Phys. Rev. Lett. 96 (2006) 220201. `doi:10.1103/PhysRevLett.96.220201.`
URL `https://link.aps.org/doi/10.1103/PhysRevLett.96.220201`

[21] S. Yanchuk, M. Wolfrum, A multiple time scale approach to the stability of external cavity modes in the Lang-Kobayashi system using the limit of large delay, SIAM Journal on Applied Dynamical Systems 9 (2) (2010) 519–535. `arXiv:https://doi.org/10.1137/090751335`, `doi:10.1137/090751335`.
URL `https://doi.org/10.1137/090751335`

[22] S. Yanchuk, G. Giacomelli, Spatio-temporal phenomena in complex systems with time delays, Journal of Physics A: Mathematical and Theoretical 50 (10) (2017) 103001. `doi:10.1088/1751-8121/50/10/103001`.
URL `http://stacks.iop.org/1751-8121/50/i=10/a=103001?key=crossref.f760c062e912b820ac69c9174ac61305`

[23] R. Mirollo, S. Strogatz, The spectrum of the partially locked state for the Kuramoto model, J Nonlinear Sci 17 (2007) 309–347. `doi:10.1007/s00332-006-0806-x`.
URL `https://doi.org/10.1007/s00332-006-0806-x`

[24] R. Lang, K. Kobayashi, External optical feedback effects on semiconductor injection laser properties, IEEE J. Quantum Electron. 16 (1980) 347–355.

[25] E. Montbrió, D. Pazó, J. Schmidt, Time delay in the Kuramoto model with bimodal frequency distribution, Phys. Rev. E 74 (2006) 056201. `doi:10.1103/PhysRevE.74.056201`.
URL `https://link.aps.org/doi/10.1103/PhysRevE.74.056201`

[26] O. E. Omel'chenko, M. Wolfrum, Nonuniversal transitions to synchrony in the Sakaguchi-Kuramoto model, Phys. Rev. Lett. 109 (2012) 164101. `doi:10.1103/PhysRevLett.109.164101`.
URL `https://link.aps.org/doi/10.1103/PhysRevLett.109.164101`

[27] O. E. Omel'chenko, M. Wolfrum, Bifurcations in the Sakaguchi-Kuramoto model, Physica D: Nonlinear Phenomena 263 (2013) 74 – 85. `doi:https://doi.org/10.1016/j.physd.2013.08.004`.
URL `http://www.sciencedirect.com/science/article/pii/S016727891300239X`

[28] O. E. Omel'chenko, M. Wolfrum, Is there an impact of small phase lags in the Kuramoto model?, Chaos: An Interdisciplinary Journal of Nonlinear Science 26 (9) (2016) 094806. `arXiv:https://doi.org/10.1063/1.4954217`, `doi:10.1063/1.4954217`.
URL `https://doi.org/10.1063/1.4954217`

[29] O. D'Huys, T. Jüngling, W. Kinzel, Stochastic switching in delay-coupled oscillators, Phys. Rev. E 90 (2014) 032918. `doi:10.1103/PhysRevE.90.032918`.
URL `https://link.aps.org/doi/10.1103/PhysRevE.90.032918`

[30] D. A. Wiley, S. H. Strogatz, M. K. Girvan, The size of the sync basin., Chaos 16 1 (2006) 015103.

[31] O. D'Huys, R. Vicente, J. Danckaert, I. Fischer, Amplitude and phase effects on the synchronization of delay-coupled oscillators, Chaos: An Interdisciplinary Journal of Nonlinear Science 20 (4) (2010) 043127. `arXiv:https://doi.org/10.1063/1.3518363`, `doi:10.1063/1.3518363`.
URL `https://doi.org/10.1063/1.3518363`